

RootPainter3D: Interactive-machine-learning enables rapid and accurate contouring for radiotherapy

Abraham George Smith^{1,2,*}, Jens Petersen^{1,2}, Cynthia Terrones-Campos³, Anne Kiil Berthelsen^{2,4}, Nora Jarrett Forbes^{1,2}, Sune Darkner¹, Lena Specht², and Ivan Richter Vogelius²

¹*Department of Computer Science, University of Copenhagen*

²*Department of Oncology, Rigshospitalet, University of Copenhagen*

³*Department of Infectious Diseases, Rigshospitalet, University of Copenhagen*

⁴*Department of Clinical Physiology, Rigshospitalet, University of Copenhagen*

*ags@di.ku.dk

Abstract

Organ-at-risk contouring is still a bottleneck in radiotherapy, with many deep learning methods falling short of promised results when evaluated on clinical data. We investigate the accuracy and time-savings resulting from the use of an interactive-machine-learning method for an organ-at-risk contouring task. We compare the method to the Eclipse contouring software and find strong agreement with manual delineations, with a dice score of 0.95. The annotations created using corrective-annotation also take less time to create as more images are annotated, resulting in substantial time savings compared to manual methods, with hearts that take 2 minutes and 2 seconds to delineate on average, after 923 images have been delineated, compared to 7 minutes and 1 seconds when delineating manually. Our experiment demonstrates that interactive-machine-learning with corrective-annotation provides a fast and accessible way for non computer-scientists to train deep-learning models to segment their own structures of interest as part of routine clinical workflows.

Source code is available at [this HTTPS URL](https://github.com/RootPainter3D).

Introduction

Half of all cancer patients receive radiotherapy [13], which is associated with a range of dose dependent

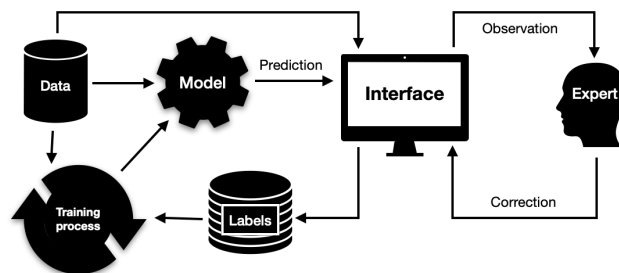


Figure 1: Interactive machine learning with corrective annotation puts the human-in-the-loop during the model training process.

side effects [4]. Effective mitigation of these side effects requires accurate delineation of organs-at-risk, such as the heart and oesophagus [17, 43]. Manual delineation is still widely used but time-consuming in comparison to automated methods [55] and subject to large inter-observer variation [37, 63]. A review of auto-segmentation methods for radiotherapy is presented by [7], indicating deep-learning methods and convolutional neural networks (CNN) in particular as representing the state-of-the-art. A survey of deep-learning for radiotherapy is presented by [44], including explanations of machine learning, deep learning, and CNNs.

Although CNNs exhibit impressive performance when the training and testing data are drawn from the same distribution [46, 34, 55, 19, 57], variations specific to on-

site clinical data may result in decreased performance [21, 20, 51]. For example [18] found that organ deformations due to an abdominal compression technique impaired the performance of an externally trained CNN model.

Training models on-site is a potential solution but can be challenging as training neural networks involves time-consuming trial and error [44] and hiring the appropriate experts is associated with high costs. A lack of large and high-quality publicly available datasets compounds the problem [59] as annotating large enough datasets for training deep-learning models with purely on-site data may be infeasible.

Corrective-annotation is an annotation sparsification strategy that results in a sub-region of each image being labelled. [65] demonstrate, using a 3D heart segmentation dataset, that annotation-sparsification allows deep-learning models to be trained using just 20% of the labelled data whilst obtaining similar performance. As opposed to [65] who rely on automatic methods to infer which regions of an image are most useful for labelling, corrective-annotation utilises human feedback (Figure 1) to identify problematic regions of the image for the model [22, 53, 29, 39]. Methods such as corrective-annotation which utilise a human-in-the-loop to improve machine learning implementations are known as interactive machine learning (IML) [31].

In prior work, corrective-annotation IML methods have been used to train deep-learning segmentation models for a diverse array of modalities, including 2D plant photographs [53, 25, 14], laser ablation tomography [16], histopathology [30] and 3D X-ray CT images of methane in sand [2].

To the best of our knowledge, no prior work has evaluated an IML approach applied to medical X-ray CT data. Therefore we implement an IML system for X-ray CT data and investigate its effectiveness for organ-at-risk segmentation.

We hypothesise that (1) semi-automatic contouring via an IML corrective-annotation method will provide similar accuracy to existing manual methods; And (2) that it will offer continuous improvements in contouring time as more images are annotated, eventually leading to significant time savings.

Method

We use a corrective-annotation approach to contour a large dataset of hearts by having a physician correct all generated contours during training (Figure 1). The process is semi-automatic, with the assisting model continuously learning as more images are annotated.

Dataset

We used X-ray CT scans from a cohort of patients that had been collated for a study on the association between mean heart dose and radiation-induced lymphopenia [56]. The CT scans were from patients who had started to receive radiotherapy to the chest region between 2009 and 2016 at Rigshospitalet in Denmark. The cohort was restricted to patients who were at least 18 years old, had dosimetric data available, a solid malignant tumour (excluding lymphoma) and a blood count both before and after receiving radiotherapy. This resulted in 933 X-ray CT scans from 923 patients, of which 308 had breast cancer, 291 had esophageal cancer, 56 had small-cell-lung-carcinoma and 268 had non-small-cell lung carcinoma. The 933 images had varying slice thicknesses. 209 images had a slice thickness of 3mm, 721 had a slice thickness of 2mm, and 3 had a slice thickness of 1mm. The number of voxels in each dimension varied. The total number of slices (depth) varied from 96 to 489 with a mean of 189. The width and height of the axial plane ranged from 512 to 658, with a mean of 537 voxels. No pre-processing was performed to normalize the images in any way. All files were saved in the gzip compressed NIfTI file format with extension .nii.gz.

Software Implementation

We implemented RootPainter3D, which is based on RootPainter, an open-source corrective-annotation software application that utilises a client-server architecture and makes the necessary operations to train and use a deep-learning model for image segmentation available via a cross-platform graphical user interface [53].

The original RootPainter uses a variant of U-Net [50] modified to utilise group norm [61] and residual connections [26]. Compared to the 2D version we modify the software in several ways. The 2D convolutional layers

were converted to 3D, resulting in a variant of the 3D U-Net architecture which is known to perform well for organ-at-risk segmentation [19] and sparse data [9]. The interface was modified to allow contrast settings to be adjusted, navigation and annotation of 3D images, with viewing enabled in both sagittal and axial views simultaneously. The data augmentation was removed. Although it is claimed data augmentation is critical to achieving favourable generalisation performance [52], results indicate the advantages of data-augmentation can be inconsistent and dataset specific [36].

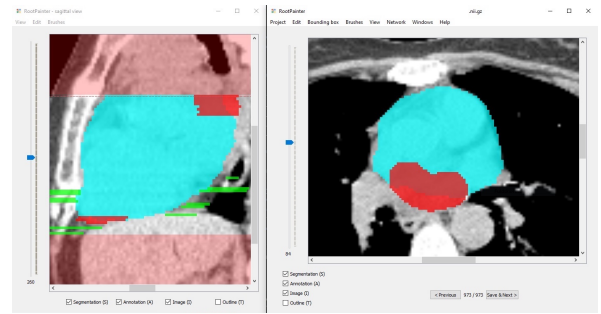
RootPainter3D allows a user to inspect model predictions on a dataset that they work through sequentially - one image at a time. For each image, they initially define a bounding box in order to obtain predictions for a region containing the organ of interest. The user is able to assign corrections to the model predictions given for the defined region. When the user clicks 'save and next' in the interface the current annotation is saved to disk in a folder of annotations which is shared with a remote server with a more powerful graphics processing unit (GPU). The server component of the software continuously trains a 3D U-Net on the available annotations using stochastic gradient descent. For RootPainter3D, batches of 4 annotations, with their associated image regions are sampled from the annotation folder without replacement. The regions of the images used for training are only those where user-annotations are assigned. Supervised training is used but the annotations are sparse. Only the defined regions (what the user has specified as either foreground or background) are used for computing the loss which is used for updating the model weights.

The contrast settings (see [Contouring procedure](#) for more details). can be changed to a preset option in the view menu, such as mediastinal, which was used for our experiments.

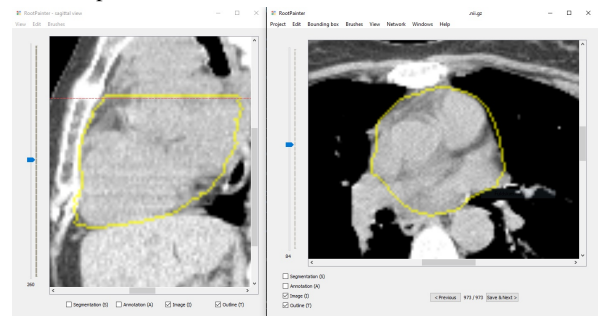
Contouring procedure

To enable comparison to a manual method widely used in the clinic, 20 hearts were also delineated using the Eclipse treatment planning software from Varian Medical Systems, Inc.

From the 933 heart CT scans, the annotator delineated the first 10 in Eclipse and then all 933 in RootPainter3D and then the last 10 in Eclipse. This was done to allow



(a) Screenshot of RootPainter3D software showing segmentation in blue and annotation in red for corrections to false negative regions and green for corrections to false positive regions. The area in light red is outside of the bounding box and is not part of the predicted or corrected region. The dashed red line shows the position of the axial slice in the sagittal view. This dashed line was added after the experiment in this study was completed based on user-feedback.



(b) Screenshot of RootPainter3D software showing the outline view with segmentation and annotation hidden.

Figure 2: Screenshots of the RootPainter3D client software. Showing different views available for heart contouring. The axial view is shown on the right and sagittal view on the left. The user is able to change what data is shown via keyboard shortcuts or with the checkboxes shown in each viewer.

the dice score to be computed between the contours done in RootPainter3D and Eclipse, and also to compare delineation time between RootPainter3D and Eclipse at the start and end of the RootPainter3D model training process.

Contouring in both Eclipse and RootPainter3D was done using the mediastinal hounsfield unit (HU) window which ranges from -125 HU to 250 HU. For both software applications, annotation can be performed in both the sagittal and axial views but for our experiment all annotation was assigned in the axial view. In RootPainter3D the user is able to view the model’s initial segmentation in blue (Figure 2a). They can annotate foreground (heart) regions in red and background (not heart) regions in green (Figure 2a). A 3D segmentation consists of a model prediction for each voxel in an image. If annotating correctively, the red foreground annotation should correspond to model predictions that were false negatives, and the green background regions should be targeted towards false positive model predictions. Taking corrections into account, the corrected contour can be viewed using the outline view (Figure 2b).

When contouring in Eclipse, every third slice was contoured and then interpolation was used to join the slices, as this is a standard clinical procedure used to save time compared to contouring all slices. The same trained physician delineated all hearts in both RootPainter3D and Eclipse using the Danish guidelines for whole heart contouring [47].

In order to ensure the physician’s familiarity with both software applications prior to the experiment, 20 hearts that were not used as part of the experiment were contoured in both applications.

Training

The training process for neural networks is a procedure where the network weights and biases are iteratively updated by a gradient descent algorithm, which compares the network outputs with the desired output [40].

When a user completes a delineation in the RootPainter3D client software, the annotation is saved to disk and training is started automatically by sending an instruction to the server.

The training routine, once started, first creates a model using Kaiming initialisation to assign random parameters

[27], and then trains that model by continuously iterating over all saved annotations.

The training procedure treats newly saved images similarly to previously saved images as all images are equally likely to be used in the next batch of the training procedure. It loads the annotations from disk and uses these, combined with the image data, to train a model to predict the annotated regions correctly. For the RootPainter3D trainer, regions that are not annotated are set to 0 in both the network predictions and annotation. This means only the regions of the image explicitly annotated as either foreground or background by the annotator are used to compute the loss. The loss is then used to update the network weights. The loss function used in RootPainter3D is a combination of cross-entropy and dice loss, taken from [54].

A GPU is required for achieving optimal performance when training large parameter models such as deep neural networks. As the entire dataset cannot fit in the memory of the GPU, stochastic gradient descent is used to make network updates based on a subset (known as a batch) of the full available dataset. In our case the network is trained with a batch size of 4. We used two NVIDIA Titan RTX GPUs, with 24GB of memory each, using a data-parallel [11] approach. Due to GPU memory constraints, instead of using the full images, a sub-region (patch) is sampled from a random location that contains annotation, from each of the randomly sampled images in the training batch. The patch dimensions are 228, 228 and 52 voxels, corresponding to width, height and depth respectively.

For the RootPainter3D trainer application, once training has started, the process is continuous, even when the client application is closed. The trainer application keeps track of a counter named *epochs_without_progress*. This counter is used to measure the length of time that the network has been trained without obtaining a new high score on the validation data.

Validation

In a machine learning context, the purpose of validation is to estimate model performance on unseen data. Networks with large capacity can overfit arbitrary datasets [64]. Fortunately, they have a tendency to learn smooth functions and overfitting can be conveniently mitigated with early stopping [8]. Early stopping involves checking model per-

formance on a portion of the data not used for training. This allows generalisation performance to be estimated and a snapshot of the model weights to be taken before overfitting has substantially degraded performance.

Similarly to 2D RootPainter [53], a portion of the annotated images are assigned to the validation set instead of the training set. The first image is assigned to the training dataset, then the second image is assigned to the validation dataset. From then on images are only assigned to the validation dataset if the training dataset is at least 5 times as large as the validation dataset.

The validation dataset is used for model selection, in a way equivalent to early stopping. An epoch typically refers to a full iteration over all available training data. In this context we define epoch length in terms of the number of examples sampled from the training data and have this automatically adjusted in relation to the validation set size, which increases as more images are annotated. If no validation images have been saved then the epoch length is 128. Otherwise the length is $\max(64, 2v)$ where v is the number of patches containing annotation in the validation set. Setting the length of the training period based on the validation set size ensures validation time does not overwhelm the training procedure, despite continuous addition of new cases.

At the end of each epoch the predictions for the model being trained are computed on the validation set and a dice score is computed using the available validation set annotations. If the model-in-training’s dice score is higher than the most recently saved model so far then it will be saved to disk and used for generating the segmentation presented to the user in the client user-interface.

epochs_without_progress will get set to 0 in two cases. Firstly, when new data is added to the training or validation datasets. Secondly, when a new model is found which obtains a new high score on the validation set.

Network training procedures are stochastic and dependent on initial weights [3]. Therefore as the first initial weights are unlikely to be optimal, repeating the training procedure with different initial weights is a simple way to obtain better results. For this reason we introduced a restart procedure. The restart procedure was not functioning for the first 478 hearts, during which the network would stop after 60 epochs without progress.

The restarting behaviour, used for the latter portion of the experiment to further boost network accuracy,

would start training the network from scratch after 60 *epochs_without_progress* were reached. If the newly trained model beat the best model on the validation set so far then it would be saved (see [Validation](#) for more details). That means if the system is left unattended for long enough, it will likely find a new best model, and keep trying relentlessly until it does.

Dice evaluation

In order to evaluate the accuracy of the RootPainter3D contours before and after user correction, we compared the dice of both the initial predicted contour and the version after corrections with contours created manually in Eclipse for the same 20 images.

For each model generated heart contour, we also compute the dice score between the predicted heart contour and corrected version for 933 images. This approach is similar to previous studies that use manually corrected model predictions as ground-truth contours for evaluation [19, 24].

Interaction logging and annotation duration

To evaluate the extent to which the trained model assisted in reducing annotation time, we asked the annotator to log the specific time periods when they started and stopped annotating. We also automatically logged interaction events with the user-interface including when the user saved an image, opened a new image, moved to a different slice in the axial or sagittal views, changed zoom settings and mouse down and mouse release events.

To compute the amount of time the annotator spent on each image, we filter to interaction events inside their manually logged annotation period. For each file, we start accumulating interaction time from when the user opens that file until they open the next file. We also exclude periods of inactivity from our duration computation, which we define as no interaction events for at least 20 seconds.

Impact on radiation dose

We also compare the computed mean heart dose (Gy) when using the initial segmentation compared to the corrected contour.

To compare dose absorption we first obtain a dose matrix for each scan from the clinical dose plan. The dose matrix provides a cumulative level of radiation dose absorbed by each voxel in the planning CT scan. We compute the mean heart dose using the dose matrix combined with both the initial segmentation and corrected structure independently. We then take the absolute difference between the two mean heart dose measurements to allow us to plot dose deviation over time as more hearts are annotated.

Results

Duration

In order to evaluate the annotation speed of RootPainter3D, we report delineation duration as a function of the number of images annotated (Figure 3). The first 10 and last 10 hearts are shown separately to highlight both the differences with Eclipse and RootPainter3D both before and after a period of extensive interactive annotation (Figure 4). RootPainter3D is initially slower and then becomes significantly faster after it has learned from more user corrections (Figure 4).

After around 110 images, delineation duration in RootPainter3D is less than the mean delineation of the 20 hearts contoured in Eclipse (Figure 3). With the exception of temporary fluctuations, the RootPainter3D per-heart delineation duration continues to decrease as more hearts are contoured (Figure 3) becoming substantially faster than the comparison manual method with the last 10 hearts taking an average of 2 minutes and 2 seconds to delineate compared to 7 minutes and 1 seconds when using Eclipse (Figure 4). The RootPainter3D delineations also maintain strong agreement with manual delineations of the same images (Table 1).

Accuracy

The dice score between the initial predicted heart and the corrected version are shown with running mean and standard deviation which were computed using a running average from 60 images (Figure 5). The dice scores of all hearts, excluding the first (which had a dice score of 0.2) are shown in figure 5. From the 300th heart onward, the vast majority of hearts have a dice score above 0.98 (Fig-

ure 7) with a few outliers having dice scores between 0.9 and 0.95 and just two extreme outliers having dice scores below 0.7 (Figure 5).

Axial slices from the outliers a and b labelled in figure 5 are illustrated in figure 6a and figure 6b respectively. These two hearts were the only ones out of the last 600 annotated which had a dice score lower than 0.9. In both cases the model appeared to be confused by a large tumour adjacent to the heart.

To show the model progression more clearly, in figure 7 the y-axis minimum is raised to 0.9, which includes most of the values. Although there are fluctuations, the mean dice score shows a trend of continuous improvement as more images are correctively delineated (Figure 7).

We found strong agreement between the hearts contoured in RootPainter3D and Eclipse (Table 1). All of the last 10 hearts in RootPainter3D had higher agreement with the manual Eclipse delineations after the corrections were assigned.

Figure 8a shows the error measured in mean dose for automatically predicted heart structure drops as more images are correctively delineated. As shown in 8b only 4 of the model predicted hearts in the last 300 result in an error in dose above 1 Gray.

Table 1: Dice scores between hearts delineated using RootPainter3D and Eclipse, showing strong agreement between methods. However, the RootPainter3D predicted and corrected contours are more similar to each other than either one is to the Eclipse contours. *pred* refers to RootPainter3D predicted contours and *cor* refers to the RootPainter3D corrected contours.

	Eclipse vs pred	Eclipse vs cor	pred vs cor
mean	0.945	0.952	0.991
std	0.008	0.007	0.005

Discussion

The strong agreement with the manual contours shown in table 1 supports our first hypothesis that RootPainter3D will result in accurate contours. Prior heart auto-contouring studies have observed a mean dice score of 0.925 between model predictions and manual delineation

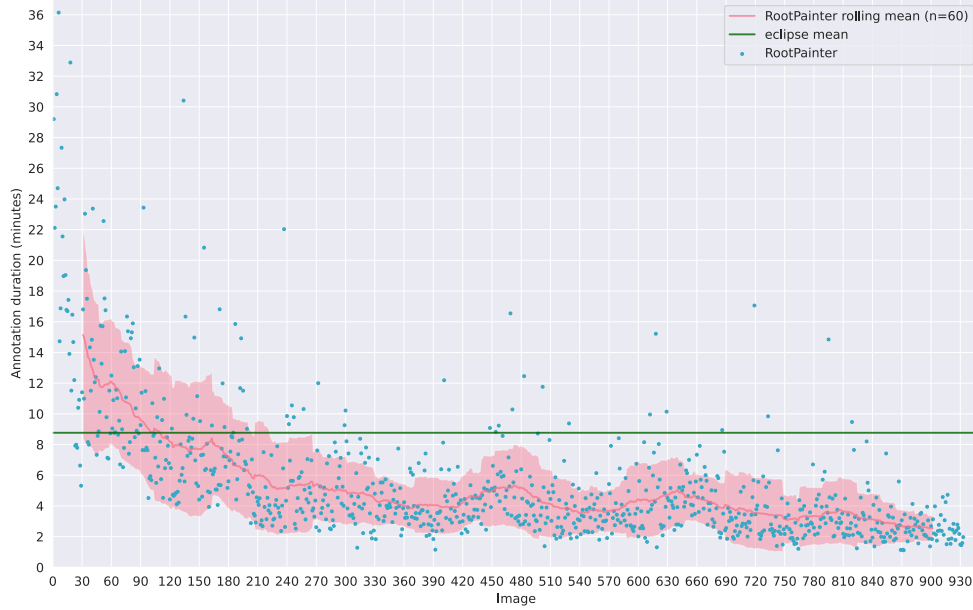


Figure 3: Delineation duration for each of the 933 images shown in order of delineation with the mean delineation duration of the 20 images contoured in Eclipse. RootPainter3D per-image delineation duration reduces over time.

[19]. [62] obtained a dice score of 0.931 when measuring the disagreement between multiple annotators, indicating the difference between RootPainter3D delineations and our manually created delineations may be less than the difference between two annotators, even before corrections are assigned.

The decrease in per-image contouring duration as more hearts are annotated (figure 3) and significantly faster contouring for the last 10 hearts (Figure 4) support our second hypothesis that RootPainter3D will offer substantial time savings.

In Eclipse, only one in every three slices was manually delineated, with the others created using interpolation. Even though in RootPainter3D all slices were manually corrected, the contouring time was still more than three times faster than Eclipse (Figure 4). This discrepancy between the number of slices delineated vs interpolated also explains why RootPainter3D was slower than eclipse during the initial period of annotation (Figure 4).

The dice scores between the RootPainter3D corrected contours and Eclipse contours are lower than the dice

scores between the RootPainter3D predicted contours and corrected contours (Table 1).

As the predicted and corrected contours are not done independently, it is expected that they will have higher agreement than two independently created contours. For quantifying errors in an existing delineation, there are some cases where this may be a strength. When delineating from scratch in noisy images and areas with little contrast, a drop in dice may be caused by differences in delineation along ambiguous border regions. With corrective-annotation, the annotator focuses on clear errors and the measured dice is therefore an indication of how often the system makes such clear errors and these may be more relevant to quantify. For creating datasets for machine learning, corrective-annotation could therefore reduce label noise consisting of natural-perturbations. Although deep-learning is relatively robust to label noise [49], perturbations along boundaries are particularly problematic for U-Net model training [28].

In prior studies, correcting contours, as opposed to contouring from scratch has been shown to increase consis-



Figure 4: RootPainter3D and Eclipse delineation duration for the first 10 and last 10 images out of the 933. RootPainter3D is initially slower than Eclipse but then becomes significantly faster. The last 10 hearts take an average of 2 minutes and 2 seconds to delineate in RootPainter3D compared to 7 minutes and 1 seconds when using Eclipse. Delineation in RootPainter3D is over three times faster than delineation in Eclipse.

tency and reduce inter-observer variation [12].

The two outliers with low dice score were in patients with anatomical abnormalities that will also likely be correlated to high dose to the heart (Figure 6). This is a potential limitation of using fully-automatic contouring for dose-response modelling and shows the importance of carefully reviewing the results of such models in clinical applications.

A typical limitation of auto-contouring studies is the small number of scans used for evaluation, with less than 100 being typical [51]. By evaluating our contouring software on over 900 hearts we were able to identify outliers that would have otherwise been missed (Figure 6). It is clear from figure 5 that smaller datasets may exclude such outliers by chance, resulting in over-optimistic characterisations of performance on unseen data.

Despite editing auto-contours being identified as a barrier to the adoption of automatic methods [62], our results, in alignment with previous studies [42, 58, 38], demonstrate that correcting auto-contours saves time compared to a standard clinical workflow. In prior work, time-

savings have been demonstrated, even when the predicted structures are of particularly low quality, with a dice score as low as 0.46 [23].

The benefits of corrective-annotation to routine clinical contouring are clear as correcting inaccurate contours is already essential to optimise treatment planning [17, 43]. In addition to being usable by non-experts [15] and providing performance improvements in comparison to fully-automated systems [32], IML can provide trust and quality control benefits [45] which are of particular interest in a radiotherapy context.

The IML process (Figure 1) provides feedback to the annotator on how much data is necessary to train a model to a given level of accuracy and due to their extended exposure to model behaviour, provides physicians with control of model training and insight into the strengths and limitations of an AI system, attributes needed to ensure clinical adoption [6].

[48] characterise IML systems as being used for task-completion or model-building. As opposed to [53], who evaluated IML with corrective-annotation for model-building, in this study we also demonstrate the potential for assisting in task-completion.

We used mean heart dose computation accuracy to measure model quality. Although it brings our results closer to a value familiar to the working radiation oncologist, the utility of mean heart dose for understanding cardiac toxicity has been called into question by recent studies [33]. With faster contouring capabilities, IML systems such as RootPainter3D provide capabilities to contour more structures in less time, making it possible to delineate organ sub-structures in a larger cohort of patients.

We motivated the omission of data-augmentation based on results that indicate the benefits may be dataset specific [36]. More recently, the same authors conducted a more thorough analysis, providing stronger indications that a sensibly designed data-augmentation procedure would provide benefits across datasets and organs [35]. Thus we expect the addition of data-augmentation would further improve our results.

Similarly to [5], we observed that many time consuming contour adjustments were minor changes along the boundary which are in many cases unlikely to have a large impact on dose. We agree with [5] that there is a need for methods that guide delineators in determining which corrections are meaningful for dose-planning.

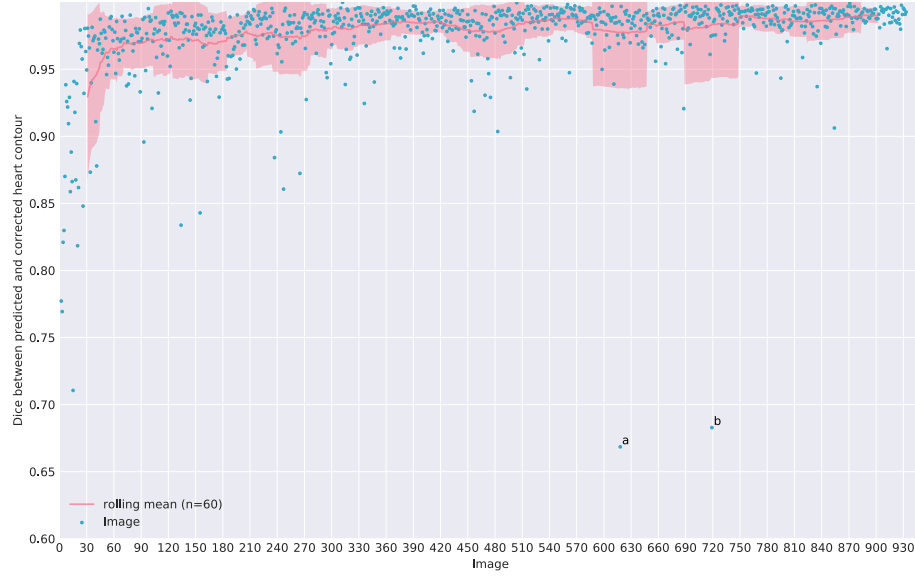
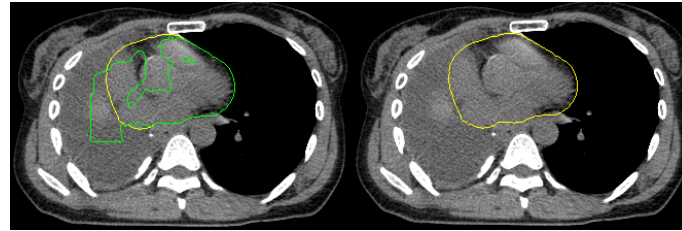
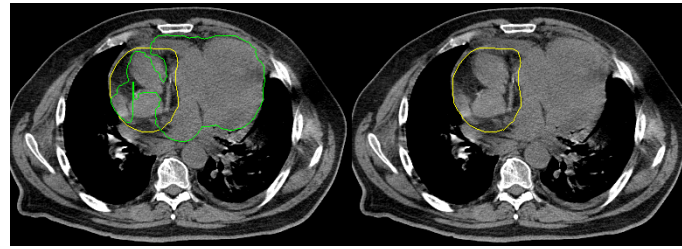


Figure 5: The dice score for 933 images shown in delineation order. After the initial training period, the vast majority of dice scores are above 0.9, with only a few outliers dropping below. Outliers are labelled a and b.



(a) Outlier a: Dice score 0.67



(b) Outlier b: Dice score 0.68.

Figure 6: Outliers a and b. For each heart two axial slices are shown with contours overlaid. On the left the model prediction is shown in green with the user corrected heart in yellow. On the right only the corrected heart is shown. For both the outliers with low dice, the tumour was located adjacent to the heart.

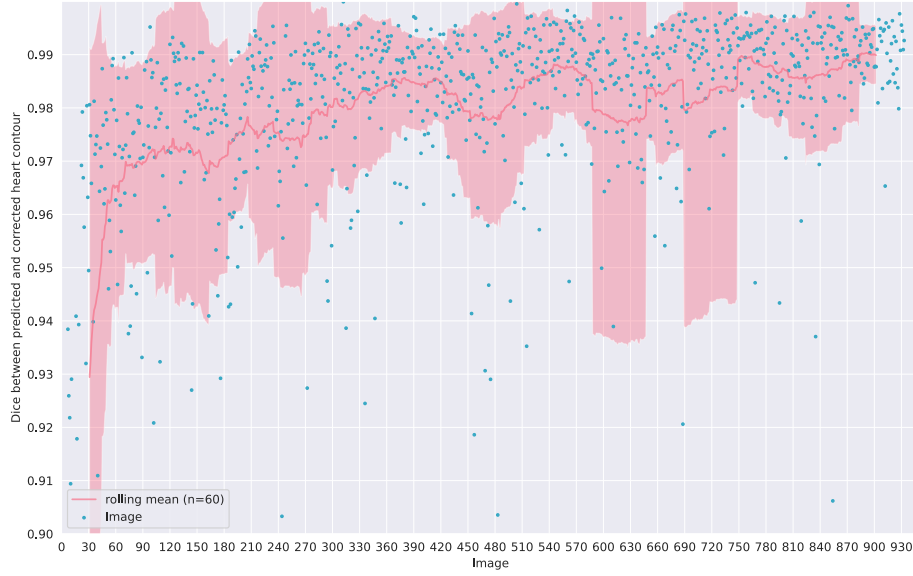
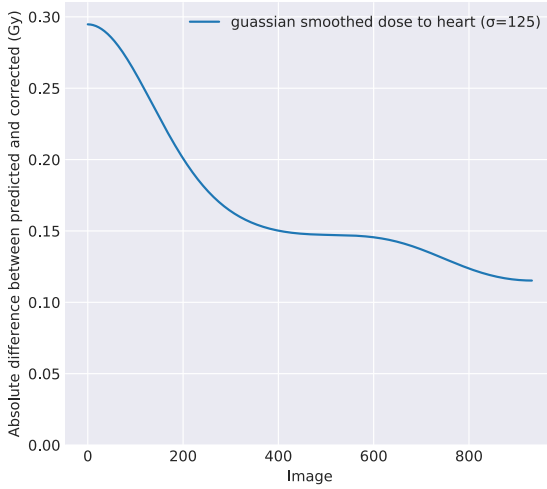
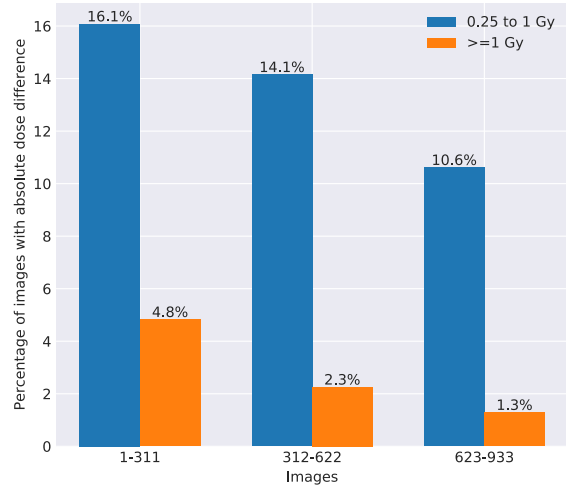


Figure 7: Dice score computed using the initial predicted image and the corrected version. Y-axis restricted to 0.9 to 1.0 to show improvement in mean over time. The mean dice score has fluctuations, but shows a general trend of improvement throughout the experiment.



(a) Running mean using a Gaussian kernel. The mean difference drops from 0.3 to 0.12 Gray as more images are correctly annotated.



(b) Percentage of hearts with absolute differences from 0.25 to 1 Gray and over 1 Gray for images 1-311, 312-622 and 623 to 923.

Figure 8: Absolute dose difference between predicted and corrected contours. The dose differences decrease as more images are annotated correctly.

The combination of electronic health records, stored dose matrices and CT scans from record and verify systems has great potential to increase our understanding of radiation dose effects for normal tissues [59]. [1] investigated the relationship between radiation exposure and lymphopenia for a cohort of 901 patients by registering all scans to a single reference patient. Our proposed method would compliment such studies by enabling efficient segmentation of structures of interest for each individual patient CT scan, potentially mitigating errors that may result from the registration process.

Our software is made available open source and we emphasise that with a restarted training process, the same application can learn to segment other organs of interest in a research setting. As we started training from random weights and use a fairly generic U-Net architecture, we expected the performance to be similar.

In conclusion, our results demonstrate the benefits of continual-learning with correction-annotation, by showing how contouring time can be continually reduced whilst maintaining accuracy. It may be some time before such systems can be made widely available to clinics, as medical devices utilising continual-learning are yet to be approved by the FDA [41, 10].

We also only used a single physician for our experiments and the contours were collected for research purposes, rather than as part of a routine procedure. The risks when working with new data and multiple clinicians will need to be carefully considered before such systems can be adopted in the clinic, and new tests may need to be designed to ensure robustness and quality [60].

Acknowledgements

We thank Thomas Carlslund and Kurt Nielsen for IT infrastructure support and Agata Wlaszczyk for proof-reading. We would also like to thank Katrin Elisabet Håkansson, Mirjana Josipovic and Emmanouil Terzidi for feedback on early versions of the software and Deborah Anne Schut for feedback on the heart contouring procedure. We also thank Mikkel Skaarup for feedback on experimental design and gratefully acknowledge our financial support from Varian Medical Systems and the Danish Cancer Society (grant no R231-A13976).

References

- [1] A. Abravan, C. Faivre-Finn, J. Kennedy, A. McWilliam, and M. van Herk. Radiotherapy-Related Lymphopenia Affects Overall Survival in Patients With Lung Cancer. *Journal of Thoracic Oncology: Official Publication of the International Association for the Study of Lung Cancer*, 15(10):1624–1635, Oct. 2020.
- [2] F. J. Alvarez-Borges, O. N. F. King, B. Madhusudhan, T. Connolley, M. Basham, and S. I. Ahmed. U-Net Segmentation Methods for Variable-Contrast XCT Images of Methane-Bearing Sand. Preprint, Soil Science, Apr. 2021.
- [3] A. Atiya and C. Ji. How initial conditions affect generalization performance in large networks. *IEEE Transactions on Neural Networks*, 8(2):448–451, Mar. 1997.
- [4] L. Barazzuol, R. P. Coppes, and P. van Luijk. Prevention and treatment of radiotherapy-induced side effects. *Molecular Oncology*, 14(7):1538–1554, 2020.
- [5] C. L. Brouwer, D. Boukerroui, J. Oliveira, P. Looney, R. J. H. M. Steenbakkers, J. A. Langendijk, S. Both, and M. J. Gooding. Assessment of manual adjustment performed in clinical practice following deep learning contouring for head and neck organs at risk in radiotherapy. *Physics and Imaging in Radiation Oncology*, 16:54–60, Oct. 2020.
- [6] C. J. Cai, S. Winter, D. Steiner, L. Wilcox, and M. Terry. "Hello AI": Uncovering the Onboarding Needs of Medical Practitioners for Human-AI Collaborative Decision-Making. *Proceedings of the ACM on Human-Computer Interaction*, 3(CSCW):104:1–104:24, Nov. 2019.
- [7] C. E. Cardenas, J. Yang, B. M. Anderson, L. E. Court, and K. B. Brock. Advances in Auto-Segmentation. *Seminars in Radiation Oncology*, 29(3):185–197, July 2019.

- [8] R. Caruana, S. Lawrence, and C. L. Giles. Overfitting in Neural Nets: Backpropagation, Conjugate Gradient, and Early Stopping. page 7.
- [9] Ö. Çiçek, A. Abdulkadir, S. S. Lienkamp, T. Brox, and O. Ronneberger. 3D U-Net: Learning Dense Volumetric Segmentation from Sparse Annotation. In S. Ourselin, L. Joskowicz, M. R. Sabuncu, G. Unal, and W. Wells, editors, *Medical Image Computing and Computer-Assisted Intervention – MICCAI 2016*, Lecture Notes in Computer Science, pages 424–432, Cham, 2016. Springer International Publishing.
- [10] S. Cruz Rivera, X. Liu, A.-W. Chan, A. K. Denniston, M. J. Calvert, SPIRIT-AI and CONSORT-AI Working Group, SPIRIT-AI and CONSORT-AI Steering Group, and SPIRIT-AI and CONSORT-AI Consensus Group. Guidelines for clinical trial protocols for interventions involving artificial intelligence: The SPIRIT-AI extension. *Nature Medicine*, 26(9):1351–1363, Sept. 2020.
- [11] J. Dean, G. Corrado, R. Monga, K. Chen, M. Devin, M. Mao, M. Ranzato, A. Senior, P. Tucker, K. Yang, Q. V. Le, and A. Y. Ng. Large Scale Distributed Deep Networks. page 9.
- [12] M. A. Deeley, A. Chen, R. D. Datteri, J. Noble, A. Cmelak, E. Donnelly, A. Malcolm, L. Moretti, J. Jaboin, K. Niernann, E. S. Yang, D. S. Yu, and B. M. Dawant. Segmentation editing improves efficiency while reducing inter-expert variation and maintaining accuracy for normal brain tissues in the presence of space-occupying lesions. *Physics in Medicine and Biology*, 58(12):4071–4097, June 2013.
- [13] G. Delaney, S. Jacob, C. Featherstone, and M. Barton. The role of radiotherapy in cancer treatment. *Cancer*, 104(6):1129–1137, 2005.
- [14] R. F. Denison. Legume-imposed selection for more-efficient symbiotic rhizobia. *Proceedings of the National Academy of Sciences*, 118(22):e2107033118, June 2021.
- [15] J. J. Dudley and P. O. Kristensson. A Review of User Interface Design for Interactive Machine Learning. *ACM Transactions on Interactive Intelligent Systems*, 8(2):8:1–8:37, June 2018.
- [16] B. Elias, A. Lanba, J. C. Netto, F. Fritschi, and A. Smith. Interactive Machine Learning Methods for the Quantification of Vascular Features in Soybean Images Obtained via Laser Ablation Tomography (LATscan). *Thinking Matters Symposium*, Apr. 2021.
- [17] G. A. Ezzell, J. M. Galvin, D. Low, J. R. Palta, I. Rosen, M. B. Sharpe, P. Xia, Y. Xiao, L. Xing, C. X. Yu, IMRT subcommittee, and AAPM Radiation Therapy committee. Guidance document on delivery, treatment planning, and clinical implementation of IMRT: Report of the IMRT Subcommittee of the AAPM Radiation Therapy Committee. *Medical Physics*, 30(8):2089–2115, Aug. 2003.
- [18] X. Feng, M. E. Bernard, T. Hunter, and Q. Chen. Improving accuracy and robustness of deep convolutional neural network based thoracic OAR segmentation. *Physics in Medicine & Biology*, 65(7):07NT01, Mar. 2020.
- [19] X. Feng, K. Qing, N. J. Tustison, C. H. Meyer, and Q. Chen. Deep convolutional neural network for segmentation of thoracic organs-at-risk using cropped 3D images. *Medical Physics*, 46(5):2169–2180, 2019.
- [20] M. Ghafoorian, A. Mehrtash, T. Kapur, N. Karssemeijer, E. Marchiori, M. Pesteie, C. R. G. Guttmann, F.-E. de Leeuw, C. M. Tempny, B. van Ginneken, A. Fedorov, P. Abolmaesumi, B. Platel, and W. M. Wells III. Transfer Learning for Domain Adaptation in MRI: Application in Brain Lesion Segmentation. *arXiv:1702.07841 [cs]*, 10435:516–524, 2017.
- [21] E. Gibson, Y. Hu, N. Ghavami, H. U. Ahmed, C. Moore, M. Emberton, H. J. Huisman, and D. C. Barratt. Inter-site Variability in Prostate Segmentation Accuracy Using Deep Learning. In A. F. Frangi, J. A. Schnabel, C. Davatzikos, C. Alberola-López, and G. Fichtinger, editors, *Medical Image Computing and Computer Assisted Intervention – MICCAI 2018*, Lecture Notes in Computer Science, pages

- 506–514, Cham, 2018. Springer International Publishing.
- [22] F. Gonda, V. Kaynig, T. R. Jones, D. Haehn, J. W. Lichtman, T. Parag, and H. Pfister. ICON: An interactive approach to train deep neural networks for segmentation of neuronal structures. In *2017 IEEE 14th International Symposium on Biomedical Imaging (ISBI 2017)*, pages 327–331, Apr. 2017.
 - [23] M. J. Gooding, A. J. Smith, M. Tariq, P. Aljabar, D. Peressutti, J. van der Stoep, B. Reymen, D. Emans, D. Hattu, J. van Loon, M. de Rooy, R. Wanders, S. Peeters, T. Lustberg, J. van Soest, A. Dekker, and W. van Elmp. Comparative evaluation of autocontouring in clinical practice: A practical method using the Turing test. *Medical Physics*, 45(11):5105–5115, 2018.
 - [24] C. Gros, B. De Leener, A. Badji, J. Maranzano, D. Eden, S. M. Dupont, J. Talbott, R. Zhuoquiong, Y. Liu, T. Granberg, R. Ouellette, Y. Tachibana, M. Hori, K. Kamiya, L. Chougar, L. Stawiarz, J. Hillert, E. Bannier, A. Kerbrat, G. Edan, P. Labauge, V. Callot, J. Pelletier, B. Audoin, H. Rasoanandrianina, J.-C. Brisset, P. Valsasina, M. A. Rocca, M. Filippi, R. Bakshi, S. Tauhid, F. Prados, M. Yiannakas, H. Kearney, O. Ciccirelli, S. Smith, C. A. Treaba, C. Mainero, J. Lefeuvre, D. S. Reich, G. Nair, V. Auclair, D. G. McLaren, A. R. Martin, M. G. Fehlings, S. Vahdat, A. Khatibi, J. Doyon, T. Shepherd, E. Charlson, S. Narayanan, and J. Cohen-Adad. Automatic segmentation of the spinal cord and intramedullary multiple sclerosis lesions with convolutional neural networks. *NeuroImage*, 184:901–915, Jan. 2019.
 - [25] E. Han, A. G. Smith, R. Kemper, R. White, J. Kirkegaard, K. Thorup-Kristensen, and M. Athmann. Digging roots is easier with AI. *bioRxiv*, page 2020.12.01.397034, Dec. 2020.
 - [26] K. He, X. Zhang, S. Ren, and J. Sun. Deep Residual Learning for Image Recognition. *arXiv:1512.03385 [cs]*, Dec. 2015.
 - [27] K. He, X. Zhang, S. Ren, and J. Sun. Delving Deep into Rectifiers: Surpassing Human-Level Performance on ImageNet Classification. *arXiv:1502.01852 [cs]*, Feb. 2015.
 - [28] N. Heller, J. Dean, and N. Papanikolopoulos. Imperfect Segmentation Labels: How Much Do They Matter? *arXiv:1806.04618 [cs]*, June 2018.
 - [29] D. J. Ho, N. P. Agaram, P. J. Schüffler, C. M. Vanderbilt, M.-H. Jean, M. R. Hameed, and T. J. Fuchs. Deep Interactive Learning: An Efficient Labeling Approach for Deep Learning-Based Osteosarcoma Treatment Response Assessment. In A. L. Martel, P. Abolmaesumi, D. Stoyanov, D. Mateus, M. A. Zuluaga, S. K. Zhou, D. Racocanu, and L. Joskowicz, editors, *Medical Image Computing and Computer Assisted Intervention – MICCAI 2020*, Lecture Notes in Computer Science, pages 540–549, Cham, 2020. Springer International Publishing.
 - [30] D. J. Ho, N. P. Agaram, P. J. Schüffler, C. M. Vanderbilt, M.-H. Jean, M. R. Hameed, and T. J. Fuchs. Deep Interactive Learning: An Efficient Labeling Approach for Deep Learning-Based Osteosarcoma Treatment Response Assessment. In A. L. Martel, P. Abolmaesumi, D. Stoyanov, D. Mateus, M. A. Zuluaga, S. K. Zhou, D. Racocanu, and L. Joskowicz, editors, *Medical Image Computing and Computer Assisted Intervention – MICCAI 2020*, Lecture Notes in Computer Science, pages 540–549, Cham, 2020. Springer International Publishing.
 - [31] A. Holzinger. Interactive machine learning for health informatics: When do we need the human-in-the-loop? *Brain Informatics*, 3(2):119–131, June 2016.
 - [32] A. Holzinger, M. Plass, M. Kickmeier-Rust, K. Holzinger, G. C. Crişan, C.-M. Pintea, and V. Palade. Interactive machine learning: Experimental evidence for the human in the algorithmic loop. *Applied Intelligence*, 49(7):2401–2414, July 2019.
 - [33] B. S. Hoppe, J. E. Bates, N. P. Mendenhall, C. G. Morris, D. Louis, M. W. Ho, R. T. Hoppe, M. Shaikh, Z. Li, and S. Flampouri. The Meaningless Meaning of Mean Heart Dose in Mediastinal Lymphoma in the Modern Radiation Therapy

- Era. *Practical Radiation Oncology*, 10(3):e147–e154, May 2020.
- [34] B. Ibragimov and L. Xing. Segmentation of organs-at-risks in head and neck CT images using convolutional neural networks. *Medical Physics*, 44(2):547–557, 2017.
- [35] F. Isensee, P. F. Jaeger, S. A. A. Kohl, J. Petersen, and K. H. Maier-Hein. nnU-Net: A self-configuring method for deep learning-based biomedical image segmentation. *Nature Methods*, 18(2):203–211, Feb. 2021.
- [36] F. Isensee, J. Petersen, S. A. A. Kohl, P. F. Jager, and K. H. Maier-Hein. nnU-Net: Breaking the Spell on Successful Medical Image Segmentation. page 9.
- [37] L. Joskowicz, D. Cohen, N. Caplan, and J. Sosna. Inter-observer variability of manual contour delineation of structures in CT. *European Radiology*, 29(3):1391–1399, Mar. 2019.
- [38] K. Kiser, A. Barman, S. Stieb, C. D. Fuller, and L. Giancardo. Novel Autosegmentation Spatial Similarity Metrics Capture the Time Required to Correct Segmentations Better than Traditional Metrics in a Thoracic Cavity Segmentation Workflow. Preprint, *Radiology and Imaging*, May 2020.
- [39] T. Kontogianni, M. Gygli, J. Uijlings, and V. Ferrari. Continuous Adaptation for Interactive Object Segmentation by Learning from Corrections. In A. Vedaldi, H. Bischof, T. Brox, and J.-M. Frahm, editors, *Computer Vision – ECCV 2020*, Lecture Notes in Computer Science, pages 579–596, Cham, 2020. Springer International Publishing.
- [40] Y. LeCun, Y. Bengio, and G. Hinton. Deep learning. *Nature*, 521(7553):436–444, May 2015.
- [41] C. S. Lee and A. Y. Lee. Clinical applications of continual learning machine learning. *The Lancet Digital Health*, 2(6):e279–e281, June 2020.
- [42] T. Lustberg, J. van Soest, M. Gooding, D. Peresutti, P. Aljabar, J. van der Stoep, W. van Elmpt, and A. Dekker. Clinical evaluation of atlas and deep learning based automatic contouring for lung cancer. *Radiotherapy and Oncology*, 126(2):312–317, Feb. 2018.
- [43] T. R. Mackie, J. Kapatoes, K. Ruchala, W. Lu, C. Wu, G. Olivera, L. Forrest, W. Tome, J. Welsh, R. Jeraj, P. Harari, P. Reckwerdt, B. Paliwal, M. Ritter, H. Keller, J. Fowler, and M. Mehta. Image guidance for precise conformal radiotherapy. *International Journal of Radiation Oncology, Biology, Physics*, 56(1):89–105, May 2003.
- [44] P. Meyer, V. Noblet, C. Mazzara, and A. Lallement. Survey on deep learning for radiotherapy. *Computers in Biology and Medicine*, 98:126–146, July 2018.
- [45] C. J. Michael, D. Acklin, and J. Scheuerman. On Interactive Machine Learning and the Potential of Cognitive Feedback. *arXiv:2003.10365 [cs]*, Mar. 2020.
- [46] F. Milletari, N. Navab, and S.-A. Ahmadi. V-Net: Fully Convolutional Neural Networks for Volumetric Medical Image Segmentation. *arXiv:1606.04797 [cs]*, June 2016.
- [47] M. L. H. Milo, B. V. Offersen, T. Bechmann, A. C. P. Diederichsen, C. R. Hansen, E. Holtved, M. Josipovic, T. Lörincz, M. V. Maraldo, M. H. Nielsen, M. Nordsmark, P. W. Nyström, M. Pøhl, H. K. Rose, T. Schytte, E. S. Yates, and E. L. Lorenzen. Delineation of whole heart and substructures in thoracic radiation therapy: National guidelines and contouring atlas by the Danish Multidisciplinary Cancer Groups. *Radiotherapy and Oncology*, 150:121–127, Sept. 2020.
- [48] G. Ramos, C. Meek, P. Simard, J. Suh, and S. Ghorashi. Interactive machine teaching: A human-centered approach to building machine-learned models. *Human-Computer Interaction*, 35(5-6):413–451, Nov. 2020.
- [49] D. Rolnick, A. Veit, S. Belongie, and N. Shavit. Deep Learning is Robust to Massive Label Noise. *arXiv:1705.10694 [cs]*, Feb. 2018.

- [50] O. Ronneberger, P. Fischer, and T. Brox. U-Net: Convolutional Networks for Biomedical Image Segmentation. In N. Navab, J. Hornegger, W. M. Wells, and A. F. Frangi, editors, *Medical Image Computing and Computer-Assisted Intervention – MICCAI 2015*, volume 9351, pages 234–241. Springer International Publishing, Cham, 2015.
- [51] J. Schreier, F. Attanasi, and H. Laaksonen. Generalization vs. Specificity: In Which Cases Should a Clinic Train its Own Segmentation Models? *Frontiers in Oncology*, 10, 2020.
- [52] P. Schwöbel, F. Warburg, M. Jørgensen, K. H. Madsen, and S. Hauberg. Probabilistic Spatial Transformers for Bayesian Data Augmentation. *arXiv:2004.03637 [cs, stat]*, Apr. 2020.
- [53] A. G. Smith, E. Han, J. Petersen, N. A. F. Olsen, C. Giese, M. Athmann, D. B. Dresbøll, and K. Thorup-Kristensen. RootPainter: Deep Learning Segmentation of Biological Images with Corrective Annotation. *bioRxiv*, page 2020.04.16.044461, May 2020.
- [54] A. G. Smith, J. Petersen, R. Selvan, and C. R. Rasmussen. Segmentation of roots in soil with U-Net. *Plant Methods*, 16(1):13, Feb. 2020.
- [55] H. Tang, X. Chen, Y. Liu, Z. Lu, J. You, M. Yang, S. Yao, G. Zhao, Y. Xu, T. Chen, Y. Liu, and X. Xie. Clinically applicable deep learning framework for organs at risk delineation in CT images. *Nature Machine Intelligence*, 1(10):480–491, Oct. 2019.
- [56] C. Terrones-Campos, B. Ledergerber, N. Forbes, A. G. Smith, M. Helleberg, J. Lundgren, L. Specht, and I. R. Vogelius. Prediction of radiation-induced lymphopenia following exposure of the thoracic region and associated risk of infections and mortality. *submitted*.
- [57] H. Um, J. Jiang, M. Thor, A. Rimner, L. Luo, J. O. Deasy, and H. Veeraraghavan. Multiple resolution residual network for automatic thoracic organs-at-risk segmentation from CT. *arXiv:2005.13690 [cs, eess]*, May 2020.
- [58] F. Vaassen, C. Hazelaar, A. Vaniqui, M. Gooding, B. van der Heyden, R. Canters, and W. van Elmpt. Evaluation of measures for assessing time-saving of automatic organ-at-risk segmentation in radiotherapy. *Physics and Imaging in Radiation Oncology*, 13:1–6, Jan. 2020.
- [59] I. R. Vogelius, J. Petersen, and S. M. Bentzen. Harnessing data science to advance radiation oncology. *Molecular Oncology*, 14(7):1514–1528, 2020.
- [60] K. N. Vokinger, S. Feuerriegel, and A. S. Kesselheim. Continual learning in medical devices: FDA’s action plan and beyond. *The Lancet Digital Health*, 0(0), Apr. 2021.
- [61] Y. Wu and K. He. Group Normalization. In *Proceedings of the European Conference on Computer Vision (ECCV)*, pages 3–19, 2018.
- [62] J. Yang, H. Veeraraghavan, S. G. Armato, K. Farahani, J. S. Kirby, J. Kalpathy-Kramer, W. van Elmpt, A. Dekker, X. Han, X. Feng, P. Aljabar, B. Oliveira, B. van der Heyden, L. Zamdborg, D. Lam, M. Gooding, and G. C. Sharp. Autosegmentation for thoracic radiation treatment planning: A grand challenge at AAPM 2017. *Medical Physics*, 45(10):4568–4581, Oct. 2018.
- [63] J. Yang, C. Wei, L. Zhang, Y. Zhang, R. S. Blum, and L. Dong. A statistical modeling approach for evaluating auto-segmentation methods for image-guided radiotherapy. *Computerized Medical Imaging and Graphics*, 36(6):492–500, Sept. 2012.
- [64] C. Zhang, S. Bengio, M. Hardt, B. Recht, and O. Vinyals. Understanding deep learning requires rethinking generalization. *arXiv:1611.03530 [cs]*, Feb. 2017.
- [65] H. Zheng, Y. Zhang, L. Yang, C. Wang, and D. Z. Chen. An Annotation Sparsification Strategy for 3D Medical Image Segmentation via Representative Selection and Self-Training. *Proceedings of the AAAI Conference on Artificial Intelligence*, 34(04):6925–6932, Apr. 2020.